Experimental Study of Nonsteady Asymmetric Flow Around an Ogive-Cylinder at Incidence

D. Degani* and G. G. Zilliac†
NASA Ames Research Center, Moffet Field, California

Flow visualization, surface-mounted pressure transducers, and hot-wire anemometers have been used to measure the leeside vortex flowfield on an ogive-cylinder at high angles of attack. Results show that there is a high degree of flowfield unsteadiness arising from several phenomena. The phenomena include large-scale von Kármán vortex shedding, high-frequency pressure and velocity fluctuations indicative of the presence of free shear-layer vortices, and a vortex interaction. The effects of axial position, angle of attack, and wind-tunnel speed on the surface pressure and velocity in the wake were investigated.

Nomenclature

C_p	= pressure coefficient, $=(P-P_\infty)/0.5\rho_\infty U_\infty{}^2$
D	= maximum diameter of body
f	= frequency, Hz
L	= length of body
M_∞	= freestream Mach number
P_∞	= freestream pressure
Re_D	= Reynolds number based on freestream conditions and D
S	= Strouhal number, $=fD/U_\infty$
U,V,W	= mean velocity components
U_∞	= freestream velocity
x,y,z	= model coordinate system
α	= angle of attack
ρ_∞	= freestream density
ϕ	= circumferential roll angle measured from windward ray

Introduction

NUMERICAL computations[1] of laminar flows around an ogive-cylinder at large incidence (Fig. 1) indicated that the computed wake is asymmetric and also unsteady. In Ref. 1, the computations were performed using a three-dimensional, time-dependent, thin-layer, Navier-Stokes code at a 40-deg angle of attack, $Re_D = 26{,}000$, and $M_\infty = 0.2$. Initially, it was thought that the code was having convergence or stability problems, but closer examination of the solution showed that shear-layer vortices were being shed into the leeside vortex flowfield at a frequency of about 1200 Hz. Although a great deal of experimental effort has been focused on the study of flows around pointed bodies at incidence, little emphasis has been placed on the unsteady aspects of these flows. As a result, the specific details of the numerically observed unsteady flow phenomena have not been observed experimentally. This study attemps to fill this gap.

Received Aug. 5, 1988; presented as Paper 88-4330 at the AIAA Atmospheric Flight Mechanics Conference, Minneapolis, MN, Aug. 15-17, 1988; revision received Feb. 15, 1989.

*Associate Professor, on leave from Faculty on Mechanical Engineering, Technion—Israel Institute of Technology, Haifa, Israel. Member AIAA.

†Research Scientist.

Several studies,[2-8] conducted on two-dimensional and inclined cylinders of various cross-sectional shapes throughout the angle-of-attack range, have indicated that a high degree of flow unsteadiness may be present because of various phenomena. In the literature, the phenomena identified include low-frequency three-dimensional effects, asymmetry-related vortex flipping, moderate-frequency von Kármán shedding, and higher frequency transition-related phenomena. In seveal cases, combinations of the phenomena have been found to coexist.

Bloor[2] found two distinct unsteady phenomena on a two-dimensional circular cylinder. The first phenomenon was the familar von Kármán vortex shedding and the second was referred to as "transition waves." A formula was suggested that relates the von Kármán vortex-shedding frequency f_s, the transition wave frequency f_t, and the Reynolds number for two-dimensional circular cylinders.

$$f_t/f_s = 0.095(Re_D)^{0.5} \qquad 2000 \le Re_D \le 16{,}000 \qquad (1)$$

Bloor[2] also states that it was difficult to obtain two successive cycles of the von Kármán vortex shedding where the transition waves were imposed regularly and clearly.

The study of Kourta et al.[3] presents additional information concerning small-scale, shear-layer vortices on two-dimensional cylinders for Reynolds numbers ranging from $Re_D = 2000$ to 6000. Hot-wire power spectra are presented at points in the shear layer. The spectra show two peaks, the first corresponding to the von Kármán vortex shedding and a second (higher frequency) shear-layer peak. The power-law relation of Bloor[2] was validated by the measurements, but some of the results presented are questionable because the frequency of the spikelike shear-layer peak is precisely 25 Hz, which is half of the line voltage frequency. An additional study was performed using a splitter plate in an attempt to suppress the von Kármán vortex shedding. It was found that the shear layer vortices were still produced at approximately the same frequency as the no-splitter-plate case, even though the shedding in the vicinity of the cylinder was suppressed and the mean flow was altered greatly.

Investigations of Wei and Smith[4] on two-dimensional circular cylinders provide support of the transition wave results described by Bloor.[2] Using hot wires and hydrogen-bubble visualization, the authors demonstrated Bloor's power-law relation (but with a different exponent) and showed that the transition waves are highly three dimensional. They conclude that the transition waves (or what the authors term "secondary vortices") appear to result from a free-shear instability

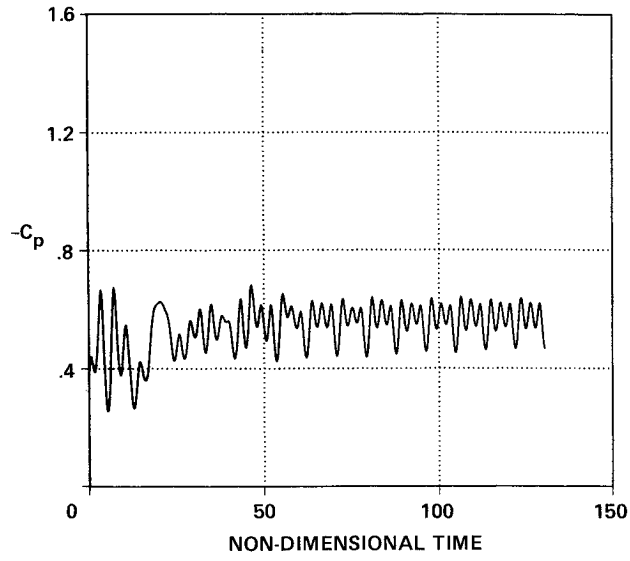

Fig. 1 Computed surface pressure coefficient history: $Re_d = 26{,}000$; $\alpha = 40$ deg; $\phi = 120$ deg; station 3; $M_\infty = 0.2$.

and that they form cellular structures, resulting in a strong spanwise mixing (a three-dimensional effect). This spanwise mixing is proposed as a mechanism that causes the von Kármán vortices to transition from laminar to turbulent.

Poll[5] investigated the flow over a long cylinder (noncircular cross section) at Reynolds numbers ranging from 4.5 to 8.3×10^5 and angles of incidence ranging from 55 to 70 deg using hot-wire anemometry and surface evaporation visualization. The main emphasis of this study was the investigation of the different types of boundary-layer instabilities and their origins. It was found that the boundary layer is susceptible to time-dependent disturbances that grow to large amplitude before the onset of transition. At the lower end of the Reynolds number range studied (prior to the transition to turbulence), a high-frequency "rider" was measured superimposed on a low-frequency, von Kármán-like wave.

Results of a study of the flow past an inclined ogive-cylinder by Dexter and Hunt[6] and Hunt and Dexter[7] showed a large-amplitude, low-frequency (less than 50 Hz) unsteadiness in the surface pressure at incidence angles between 30 and 75 deg and $Re_D = 10^5$. The mean and fluctuating surface pressure levels were found to be dependent on the freestream turbulence level. It was also demonstrated that changes in the roll angle of the nose, although maintaining a constant circumferential pressure tapping location on the cylinder, had a substantial impact on the magnitude of the mean surface pressures. The level of fluctuating surface pressures remained essentially unaffected by nose roll angle.

Ericsson[8] analyzed the results of several studies on the flow over pointed bodies of revolution at angle of attack (including the data of Hunt and Dexter[7]) and concluded that for angles less than that which produce the von Kármán vortex shedding, a vortex "flipping" could occur. Flipping was described as the intermittent changing between the two extreme asymmetric vortex geometries and is a relatively low-frequency phenomenon.

The current experimental study is a unique example of a case where the phenomenon of inerest initially was identified computationally. Although the computations were carried out on the largest computer currently available, an experimental investigation was deemed necessary to verify these findings and to explore the various aspects of the phenomena. This paper presents results of experiments examining flows around an ogive-cylinder at angles of attack ranging from 0 to 85 deg. Results show that the flowfield is unsteady, with a wide range of frequencies, even for angles of attack below 40 deg.

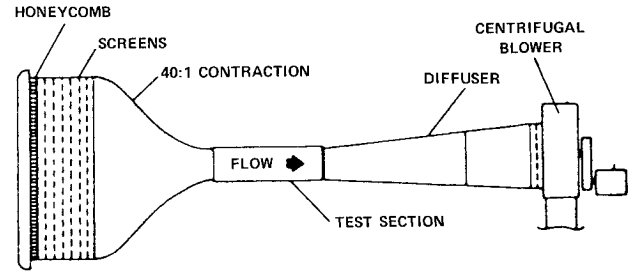

Fig. 2 15 × 15-in. low-turbulence wind tunnel.

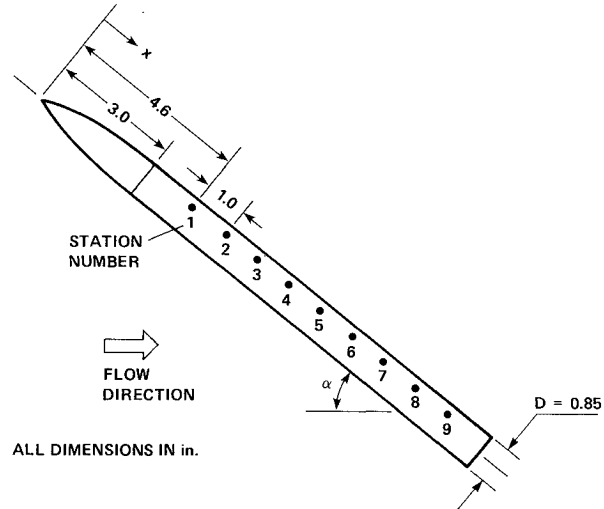

Fig. 3 Ogive-cylinder model.

Experimental Approach

Surface-pressure and wake-velocity measurements were performed in a 38 × 38-cm (15 × 15-in.), low-turbulence wind tunnel (Fig. 2) at velocities ranging from 12 to 24 m/s (40–80 ft/s). The maximum freestream turbulence level of this facility, as measured by a hot-wire anemometer, is 0.15%.

Two model configurations were studied. The first configuration consisted of an $L/D = 3.5$ tangent ogive with an $L/D = 12.5$ cylindrical afterbody (Fig. 3). The overall length of the model was 35 cm (13.75 in.), and the diameter of the cylindrical afterbody portion of the model was 2.16 cm (0.85 in.). The model was mounted rigidly on a sting support. The second configuration consisted of the same model with a splitter plate installed on the leeward plane of symmetry along the full length of the body. The splitter plate was bonded to the model surface and extended to the upper wall of the wind tunnel. The plate thickness was 0.5 mm (0.02 in.).

Pressure measurements were carried out using two Endevco model 8507C-5 pressure transducers. These transducers were mounted in Teflon holders that could be positioned in the model to measure the fluctuating pressure at one of nine longitudinal stations along the cylindrical portion of the model (Fig. 3). The first port was located at $x/D = 5.4$ from the tip, and the remaining ports were uniformly spaced ($\Delta x/D = 1.17$) downstream. Care was taken in the design of the model to minimize the volume of air between the transducer face and pressure tap to achieve the highest pressure transducer frequency response possible. Each longitudinal station consisted of two pressure taps located 90 deg apart circumferentially. The roll angle, angle of attack, and sideslip angle of the model each could be varied independently.

Primary instumentation used in the study included two channels of Newport Corporation model 2000 transducer conditioner (bride and amplification), a Krohn-Hite model 3342R filter unit, a Hewlett-Packard 3582A digital spectrum ana-

lyzer, a MicroVAX II computer with a 12-bit (analog-to-digital A/D) converter, and a DISA model 55M10 hot-wire anemometer.

The digital spectrum analyzer has an internal A/D converter that samples at a rate of 102.4 kHz. Typically, 256 records of 1024 samples each are transformed and then rms averaged to form each spectrum. The rate at which the samples are taken from the A/D converter to form the time record is a function of the frequency-span setting of the analyzer. The total number of samples used by the analyzer to compute each spectrum is approximately 250,000.

The sensitivity of the Endevco transducers was 70 mV/psi (ungained). The frequency response of the installed transducer was checked by using a 90-dB sound-level reference source and found to be greater than 10,000 Hz. The signal was amplified by a factor of 2000–10,000 to maximize the signal-to-noise ratio of the measurement system. At a gain of 2000, the wide-band noise of the measurement system was around 40 mV rms (the signal level present with no flow in the wind tunnel). Using a 25-kHz low-pass filter, the signal-to-noise ratio based on the smallest signal fluctuation of interest is greater than 25 for all of the results presented.

No boundary-layer trips were used to stabilize the vortex positions or to cause boundary-layer transition. Maximum wind-tunnel model blockage, based on the projected frontal area of the model, was less than 5.0% of the cross-sectional area of the test section at 90-deg angle of attack.

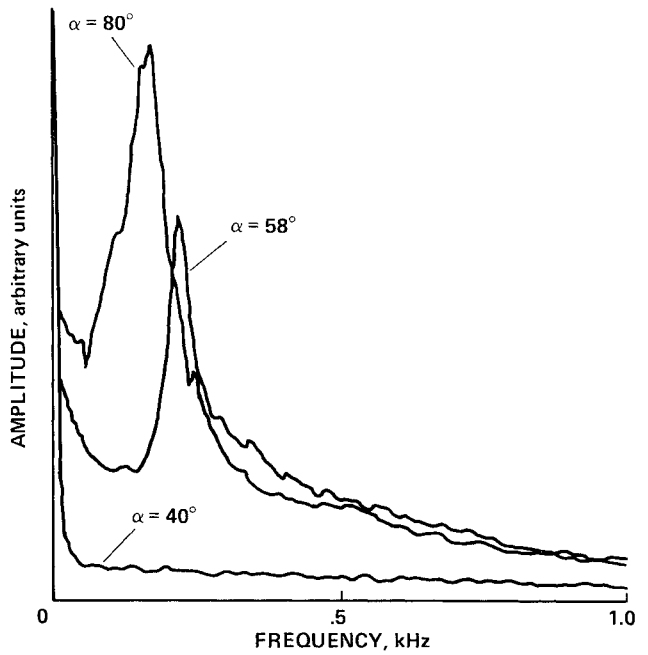

a) Hot-wire power spectra in the near wake above station 1

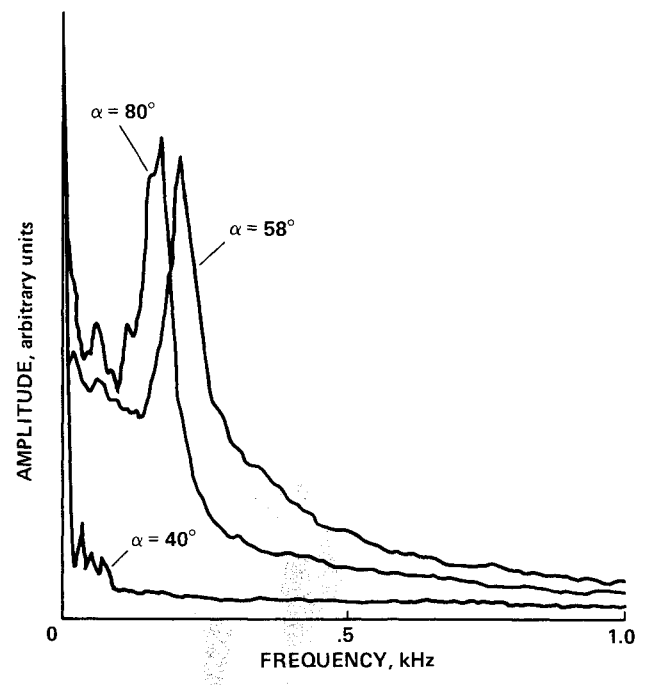

b) Surface-pressure power spectra at station 1, $\phi = 120$ deg

Fig. 4 Comparison of hot-wire and surface-pressure measurements, $Re_D = 26{,}000$.

Results

Measurements were made at three Reynolds numbers of 17,000, 26,000, and 35,000 at angles of attack ranging from 0 to 85 deg and at eight stations along the body. Pressure transducer measurements and smoke visualization showed that the flow separation was laminar and was located circumferentially approximately 90 deg from the windward ray.

Gerich and Eckelmann[9] have reported that model end conditions can have a substantial effect on the flowfield around two-dimensional circular cylinders. During the present experiment, the ogive-cylinder model was translated vertially to assess the effects of the upper wind-tunnel wall on the tip flow. No measurable effect was found at any of the angles of attack measured. Apparently, the walls have a minimal effect on the tip flow. The pressure tranducer signal does have a very low frequency component (order of 10 Hz), which is presently unexplained, but may be attributed to the presence of the wind-tunnel walls. Translation of the model away from the bottom wall of the tunnel had a minimal effect on the results shown in the following sections.

The following two subsections contain analyses of the pressure transducer signals from a time-domain and a

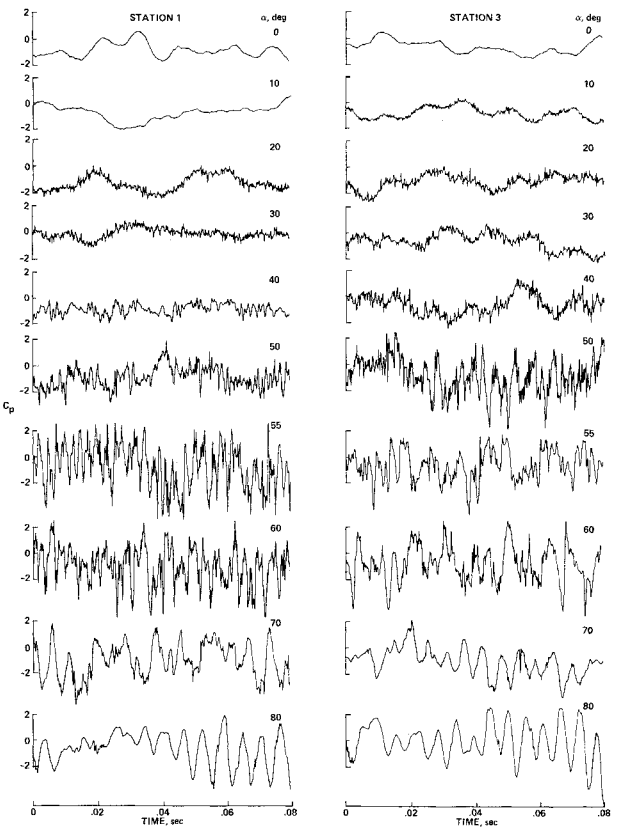

Fig. 5 Time histories of surface pressure at $Re_D = 26{,}000$, $\phi = 120$ deg.

frequency-domain point of view, respectively. Because some of the phenomena being discussed are not periodic, the frequency spectrum analysis does not always reflect all of the features that are evident in the time histories of the data. Spectral analysis involves sampling over a finite period of time, which can cause nonperiodic occurrences to be averaged out.

Some of the measurements discussed in this section were taken using a hot-wire anemometry system. Figure 4 shows power spectra obtained from both hot-wire measurements and surface-pressure measurements at several angles of attack. The pressure measurements were obtained at station 1, and the hot-wire probe was located within one body diameter above the port. As seen in Fig. 4, the basic trends of the frequency spectra of both the hot-wire and the surface-pressure data are similar when the hot-wire probe is placed in noncritical locations in proximity to the surface-pressure transducer location. However, if the probe is placed in certain highly sensitive locations (e.g., close to the ogive tip), the probe can cause the vortices to flip sides. Therefore, it was decided to rely primarily on the surface-pressure transducer measurements.

Time Domain

Figure 5 shows the effect of variation of angle of attack (0 deg $\leq \alpha \leq$ 80 deg) on the time histories of the fluctuating component of the surface pressure measured at stations 1 and 3 at $Re_D = 26{,}000$. The circumferential location of the transducer was 120 deg from the windward ray of the model.

Results indicate that the flowfield is unsteady, even at

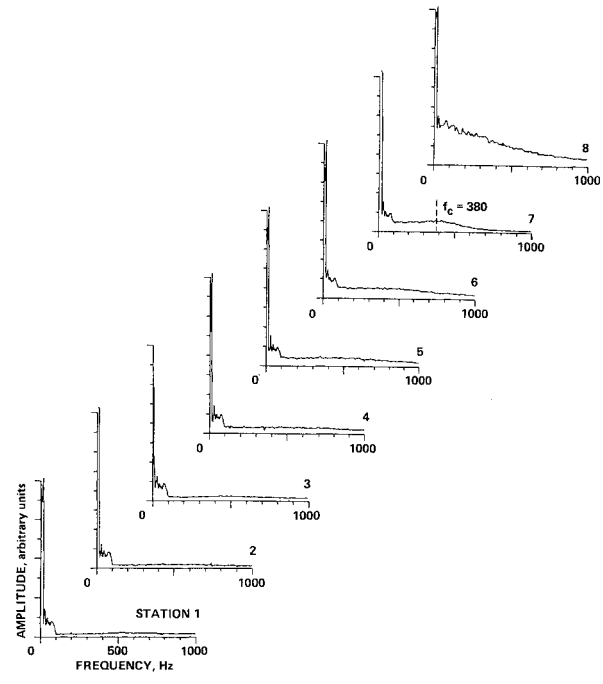

a) $\alpha = 30$ deg

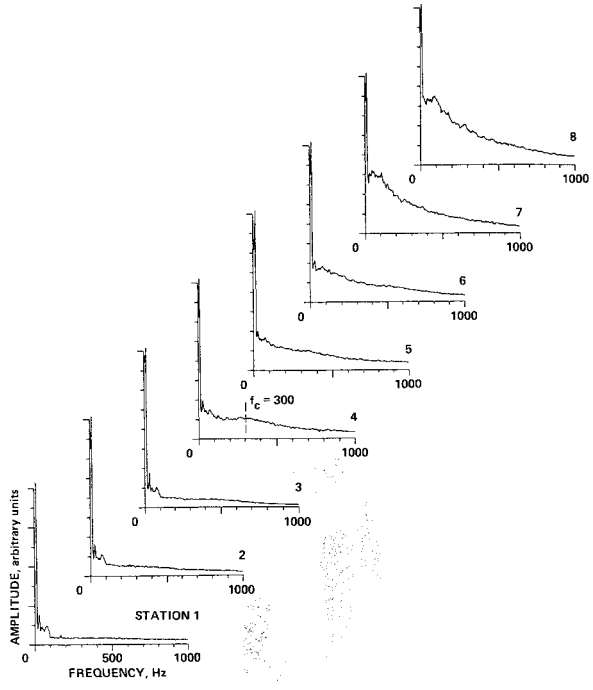

b) $\alpha = 40$ deg

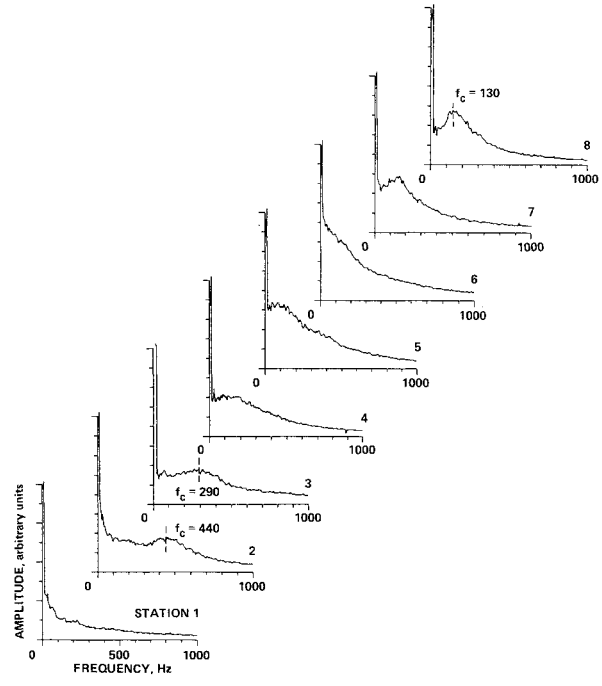

c) $\alpha = 50$ deg

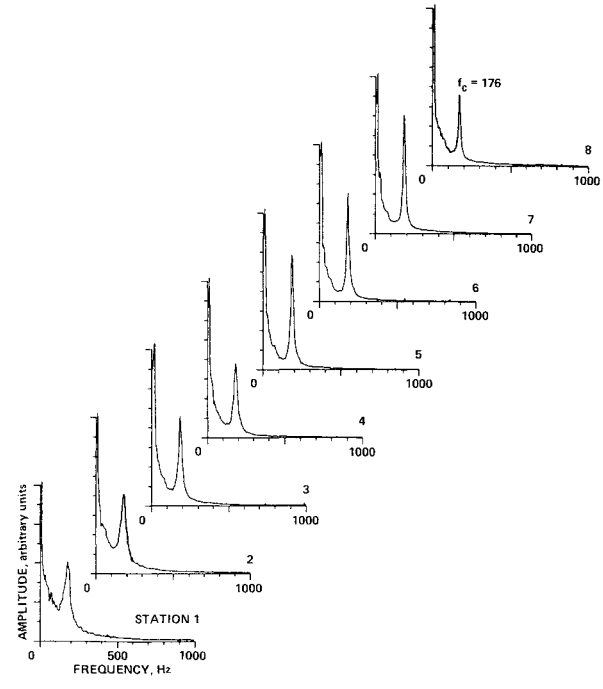

d) $\alpha = 85$ deg

Fig. 6 Effect of angle of attack on the low-frequency range of pressure power spectra at $Re_D = 26{,}000$, $\phi = 120$ deg.

moderate angles of attack (30 deg $\leq \alpha \leq$ 40 deg). It is clear that the signal has several different frequency components, and that some of the components are nonperiodic and intermittent.

At $\alpha = 30$ deg, the signal is of high frequency (1500–6000 Hz) and relatively low amplitude. As the angle of attack is increased from 30 to 40 deg, a low-frequency component (approximately 200 Hz) begins to develop. The amplitude of the high-frequency component remains relatively unchanged, but it becomes intermittent.

In general, as the angle of attack increases from 30 to 60 deg, the amplitude of both the high- and low-frequency components increases. As the angle of attack increases from 60 to 80 deg, the trend reverses itself.

Frequency Domain

Figures 6–10 present the pressure transducer power spectra (on a linear scale). Figures 6a–d show the effect of varying incidence on the low-frequency range (0–1000 Hz) of the spectra for $Re_D = 26{,}000$. Each figure contains eight curves corresponding to each longitudinal pressure tap location. It should be noted that each curve was obtained from an individual run.

For angles of attack of 30 and 40 deg (Figs. 6a and 6b), the spectra are relatively flat with no identifiable peaks above 100 Hz. However, there are indications of the incipient formation of a peak in the spectrum measured at station 7 at $\alpha = 30$ deg and in the spectrum measured at station 4 at $\alpha = 40$ deg of frequencies of about 380 and 300 Hz, respectively. At frequencies of less than 100 Hz at the first few stations, there is some small amplitude response, which is unexplained at this time. With increasing longitudinal distance (x) the energy content of the spectra increases, especially at the lower frequencies.

With an increase in angle of attack to 50 deg (Fig. 6c), three identifiable trends appear in the data. At station 2, a crest is present in the spectra, centered around 440 Hz. For stations 3–6, the center frequency of the crest decreases. At stations 7 and 8, a crest, centered at 130 Hz, is evident in the spectra. In the following sections, it will be shown that the 130-Hz crest is associated with the von Kármán vortex shedding, whereas the frequencies in the range of 300–450 Hz are associated with a separate phenomenon which we will refer to as a vortex interaction. The analogous results, obtained at angles of attack of 55 and 60 deg (not shown), have a similar behavior. The energy content of the spectra decreases and the peaks become more defined as the angle of attack increases.

The data measured at angles of attack of 70 (not shown) and 85 deg (Fig. 6d) show evidence of von Kármán vortex shedding all along the body. For the $\alpha = 70$-deg case, the peaks are at a frequency of approximately 170 Hz, and at $\alpha = 85$ deg, the shedding frequency is 176 Hz. For angles of attack of 70 deg and higher with increasing longitudinal distance and increasing angles of attack, the vortex-shedding peak becomes more defined and the energy content of the spectra decreases.

In general, although not shown, the trends observed in the power spectra with variation in angle of attack and longitudinal location are similar for the three Reynolds numbers studied. Figure 7 shows the effect of variation in tunnel velocity (Reynolds number) on the low-frequency range of the power spectra at station 2 at two angles of attack. Figure 7a presents results for an angle of attack of 50 deg, whereas the corresponding results for $\alpha = 85$ deg are shown in Fig. 7b. At $\alpha = 50$ deg, the center frequency of the main crest for each Reynolds number inceases as the tunnel velocity increases, but not in a

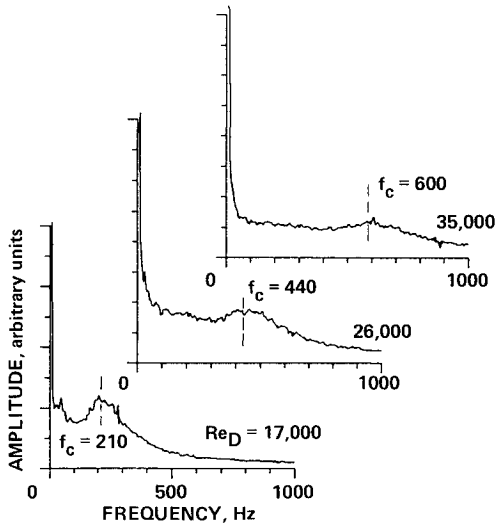

a) $\alpha = 50$ deg

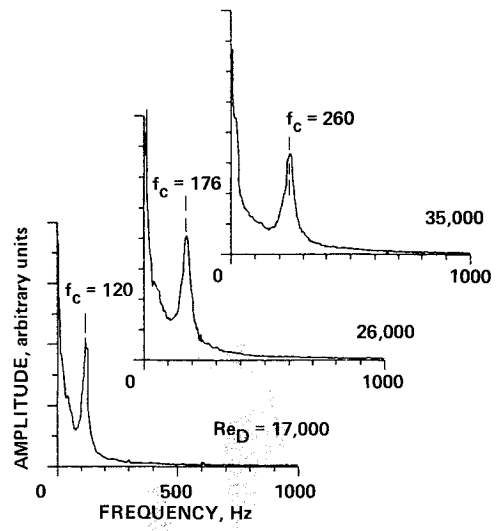

b) $\alpha = 85$ deg

Fig. 7 Effect of tunnel velocity on the low-frequency range of pressure power spectra at $Re_D = 17{,}000$, 26,000, and 35,000; $\phi = 120$ deg.

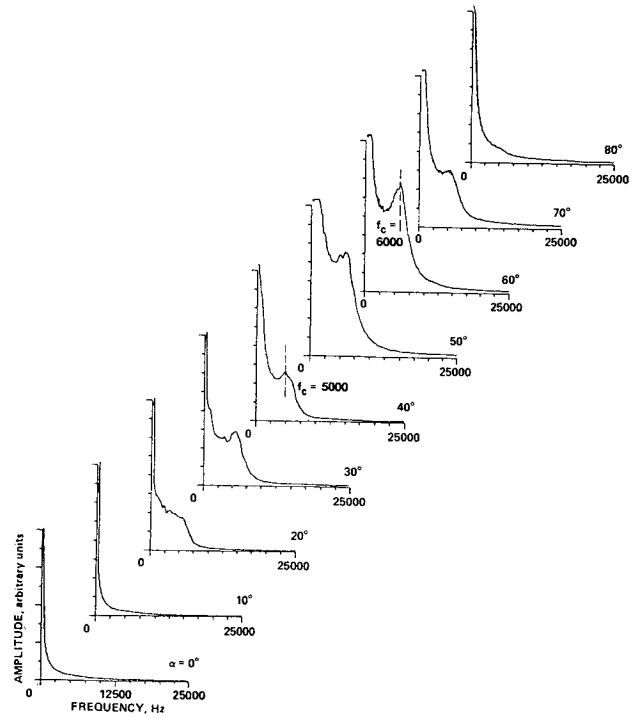

Fig. 8 Effect of angle of attack on the high-frequency range of pressure power spectra at $Re_D = 26{,}000$, $\phi = 120$ deg.

linear manner. In addition, these frequencies are higher than the von Kármán vortex-shedding frequencies that would be obtained for this angle of attack based on the crossflow velocity component. At an angle of attack of 85 deg (Fig. 7b), the frequencies of the peaks for all tunnel velocities are the von Kármán vortex-shedding frequencies and are linearly dependent on velocity.

Figure 8 shows the variation with angle of attack of the high-frequency range (0–25 kHz) of the spectra measured at station 1 for $Re_D = 26{,}000$. For angles of attack of 0 and 10 deg, there are not discernible peaks in the pressure power spectra. At 20 deg, the shape of the curve shows the initial development of a peak. As the angle of attack increases from 30 to 60 deg, the peak becomes more pronounced in the frequency range of 5000–6000 Hz. As the angle of attack increases from 70 to 80 deg, the high-frequency peak attenuates. This agrees with the trends seen in the time histories of Fig. 5, which clearly show that the high-frequency fluctuations are diminished at very low and very high angles of attack under the conditions studied. Similar trends were obtained at the other axial stations. Note that the frequency spectra shown in Figs. 6 and 7 would be located in the region to the left of the first tick mark of the horizontal axis of Fig. 8. The von Kármán vortex shedding is contained in this initial segment of the curve and is of much greater amplitude than the high-frequency pressure fluctuations.

The results obtained with the second configuration—namely, the model with the splitter plate—are shown in Figs. 9 and 10. The low-frequency-range pressure fluctuations are presented in Fig. 9, whereas the high-frequency-range spectra are shown in Fig. 10. In contrast to the results for the model without the splitter plate (Fig. 6), the low-frequency-range spectra do not show any significant peaks (aside from some low-amplitude response at frequencies less than 100 Hz). The data presented in Fig. 9 confirm that the presence of the splitter plate has suppressed the von Kármán vortex shedding. On the other hand, the high-frequency-range results presented in Fig. 10 show peaks similar to those obtained for the model without the splitter plate (Fig. 8).

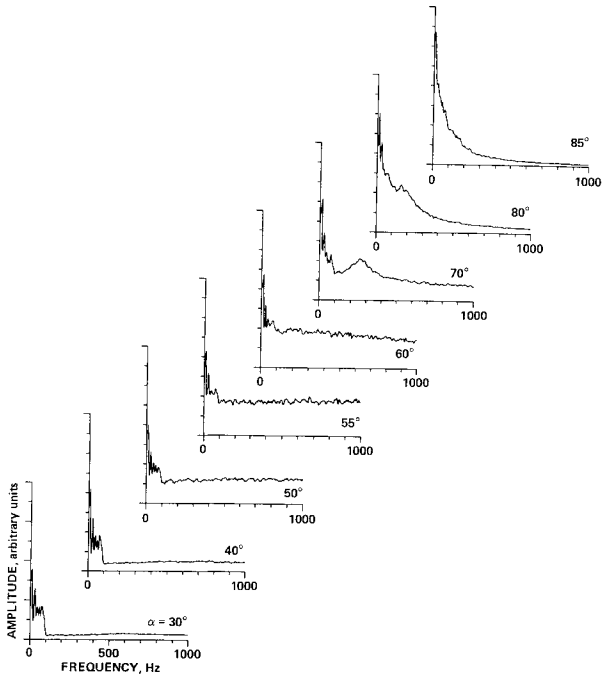

Fig. 9 Effect of splitter plate on the low-frequeny range of pressure power spectra at $Re_D = 26{,}000$, $\phi = 120$ deg.

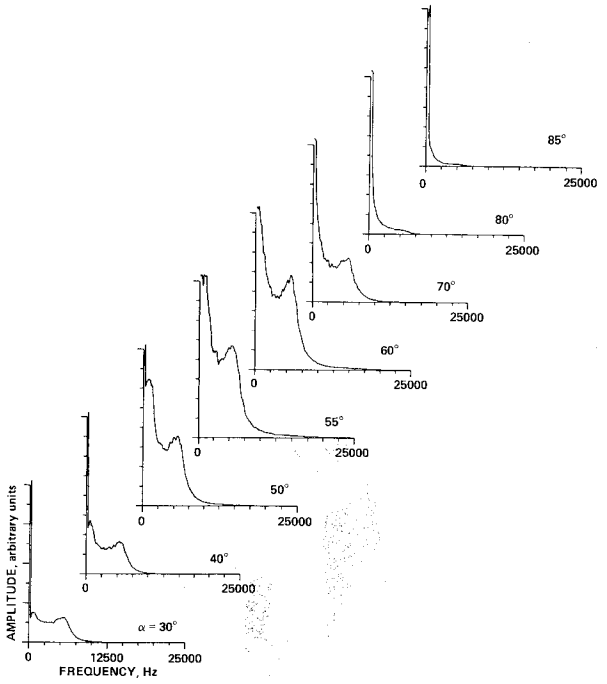

Fig. 10 Effect of splitter plate on the high-frequency range of pressure power spectra at $Re_D = 26{,}000$, $\phi = 120$ deg.

Flow Visualization

A series of high-speed movies (1500–6000 frames/s) was taken at different tunnel conditions to visualize the characteristics of the flow. A filament of smoke was introduced into the tunnel upstream of the contraction and was positioned to impinge on the tip of the model. A cross section of the flowfield was illuminated by a 4-W argon-ion laser.

Figures 11a–e show a sequence of successive frames of the flowfield cross section near station 1 at $\alpha = 55$ deg, shot at about 1500 frames/s. The black area in the photographs

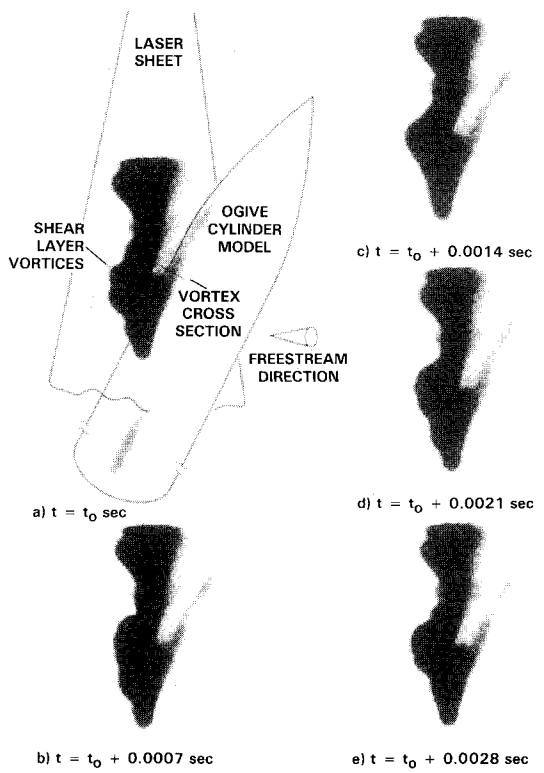

Fig. 11 Smoke-laser sheet visualization of flowfield: $Re_D = 26{,}000$; $\alpha = 55$ deg.

shows a cross section of the smoke that was entrained into the vortices at the tip. Other visualization experiments using multiple smoke filaments were performed to prove that the free shear-layer edge is indeed correctly filled out by the smoke from the tip filament.

Although it is difficult to see the details of the shape of the shear layer, a distinct waviness appears to originate near the model surface. The waves move at high speed and are neither periodic nor uniform in shape and amplitude. As shown previously in Fig. 8, the high-frequency component bandwidth is in the range of 5000–6000 Hz. These frequencies are too high to permit frame-by-frame analysis of the movement of the shear-layer vortices. However, it is important to note that the shape of the free shear layer changes significantly with time.

Discussion and Interpetation

The results presented in the previous paragraphs show that the common notion that the flowfields around slender bodies at moderate angles of attack are asymmetric but steady, is incomplete. Even at low angles of attack (30 deg $\leq \alpha \leq$ 40 deg) the flow is unsteady, containing wide ranges of amplitudes and frequencies. The results can be grouped into three types, as outlined next.

von Kármán Vortex Shedding

For angles of attack greater than 70 deg, as shown in Fig. 6d, the flow is shed from the body in a manner similar to the von Kármán votex shedding on a two-dimensional circular cylinder. Figure 12 shows the Strouhal frequency peaks of the shedding determined from the surface-pressure spectra at station 3 as a function of angle of attack. A theoretical curve given by $S = 0.21 \sin(\alpha)$ is also shown. The value of 0.21 is the classical Strouhal number of the von Kármán vortex shedding measured for a two-dimensional cylinder. It appears that the shedding frequency (f) varies with $\sin(\alpha)$ for angles of attack between 65 and 90 deg for the two tunnel velocities shown. For lower angles, it is difficult to distinguish a von Kármán vortex-shedding peak at this station. For angles of attack less than 65 deg at stations near the lower portion of the body, the presence of von Kármán vortex shedding is also evident at a Strouhal frequency corresponding to the local crossflow veloity.

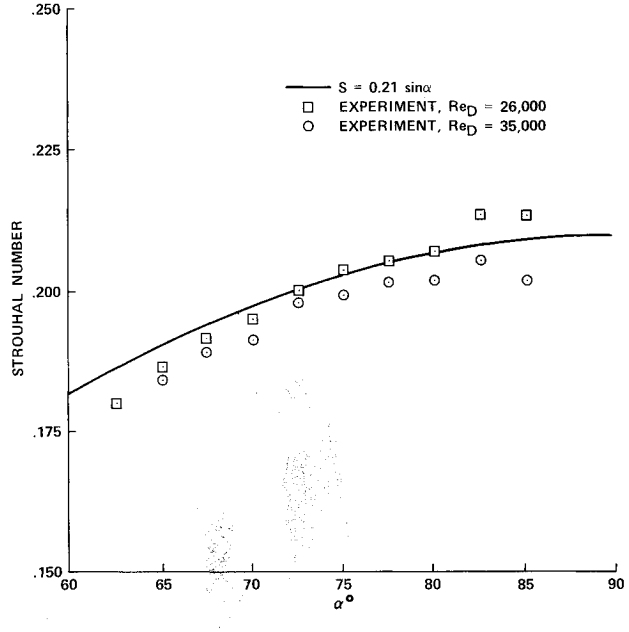

Fig. 12 Variation of the von Kármán shedding frequency with angle of attack.

Unsteadiness of Shear Layer

It is evident from the smoke-visualization photographs (Fig. 11) that the shear layer contains small-scale unsteady waves. Similarly, the pressure and velocity measurements (cf, Figs. 14 and 8) indicate that the high-frequency fluctuations are present in the separated boundary layer. This unsteadiness is a manifestation of small-scale, three-dimensional vortices present on the free-shear layer. A similar three-dimensional shear-layer vortex phenomenon was observed by Bloor,[2] Kourta et al.,[3] and Wei and Smith[4] for the case of a two-dimensional cylinder and by Poll[5] on an inclined three-dimensional cylinder. In contrast to the distinct frequency of the shear-layer unsteadiness observed in previous studies[2-4] and summarized by Eq. (1), the frequency of the high-frequency fluctuations observed in the present study varies between 1500 and 6000 Hz. The small-scale shear-layer vortices are more pronounced for angles of attack between 30 and 60 deg and appear to be independent of the large-scale von Kármán vortex-shedding phenomenon.

A demonstration of the independence of the shear-layer phenomenon from the lower frequency von Kármán vortex-shedding can be seen by comparing the data obtained with and without the splitter plate, i.e., by comparing the low-frequency-range data of Figs. 6 and 9 and the high-frequency-range data shown in Figs. 8 and 10. The low-frequency-range data (Figs. 6 and 9) show that the splitter plate suppresses the vortex shedding, whereas Figs. 8 and 10 show that the high-frequency pressure fluctuations remain basically unchanged. Because of the relatively high frequency of the shear-layer fluctuations and the observed steadiness of the primary vortex core positions (near the tip), this phenomenon is also unrelated to the low-frequency vortex-flipping phenomenon (discussed in Ref. 8). It has been suggested that the shear-layer unsteadiness is related to the Kelvin-Helmhotz instability. Nevertheless, this type of instability has not been measured previously on pointed bodies of revolution at incidence.

Vortex Interaction

Explanation of the fluctuations described earlier does not satisfactorily explain the data measured in the midsection of the body for angles of attack in the range of 30–60 deg. Under these conditions, the pressure spectra show peaks (marked on Fig. 7a) at frequencies significantly higher than the von Kármán vortex shedding (marked on Fig. 7b) but lower than the shear-layer fluctuations. The authors believe that the pressure fluctuations at these frequencies are due to an interaction between a pair of the counterrotating vortices as they curve away from the body surface and become parallel to the freestream. Figure 13 shows a schematic of the interpretation of this process. As the angle of attack is decreased from 60 deg (not shown), the location of this interaction moves farther

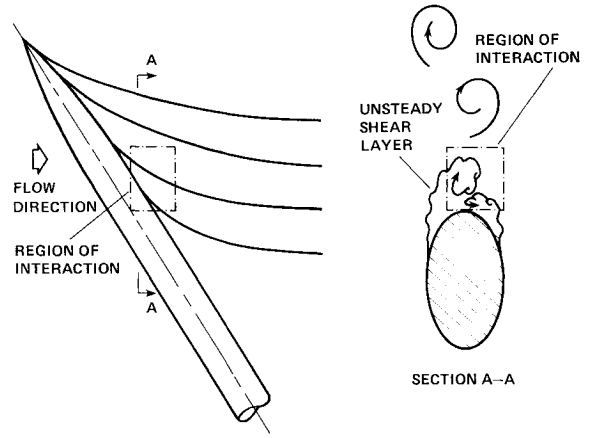

Fig. 13 Schematic of the vortex interaction $\alpha = 50$–60 deg.

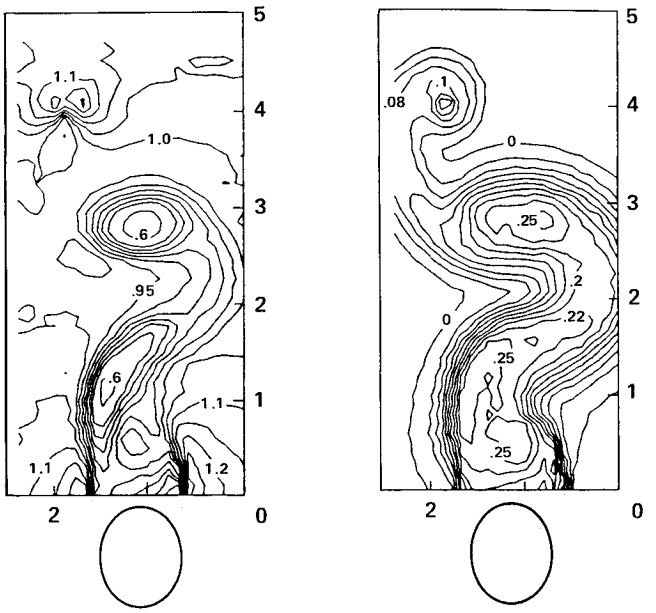

a) Mean velocity b) rms velocity

Fig. 14 Hot-wire survey of a plane at station 4: $Re_D = 26{,}000$; $\alpha = 55$ deg.

down the body. This movement coincides with the change of the location where the vortices leave the surface of the model.

In the 50–60-deg angle-of-attack range, several pairs of vortices are observed. There is limited evidence that, associated with the departure of each pair of vortices from the surface of the model, a vortex interaction zone is present.

Additional data supporting the vortex interaction interpretation are found in the hot-wire measurements. Data taken in the interaction area above station 1 at an angle of attack of 58 deg show velocity spectra similar to the pressure spectra measured at position 1 (see Fig. 4). These velocity spectra are found only in a limited volume in the vicinity of the observed interaction zone. Figure 14 shows the mean and rms velocity (kinetic energy) contours measured above station 4 (on a grid-size of 0.25 cm). The rms velocity contours indicate that, in the region of interaction (shown in Fig. 13), the magnitude of the rms velocity fluctuations is 25% of the mean velocity. These fluctuations are equal to the largest measured anywhere in the flowfield. In this region, the third and fourth counterrotating vortices, with highly distorted cross selections, are positioned closely together. It is possible that these vortices are interacting to produce the peak in the velocity spectra shown in Fig. 4a (at $\alpha = 58$ deg).

By observing the high-speed movies, it can be seen that, for all angles of attack up to 60 deg, the flow is steady in the region between the tip and the position where the tip vortices leave the surface.

Conclusions

It has been demonstrated that the flowfield around an ogive-cylinder at angles of attack above 30 deg is highly unsteady. Three distinct unsteady flow phenomena have been identified. These phenomena include low-frequency von Kármán vortex shedding, high-frequency shear-layer unsteadiness, and a vortex interaction at moderate frequency.

The von Kármán vortex-shedding frequency has been shown to vary with the crossflow velocity as the angle of attack is changed. The shear-layer fluctuations have been found to decrease in amplitude and become intermittent as the angle of attack approaches 90 deg. The vortex interaction is limited to areas where pairs of counterrotating vortices curve away from the surface of the body. There is limited evidence of the presence of more than one area of interaction along the body of a given angle of attack.

Acknowledgments

The authors would like to thank Murray Tobak and Lewis Schiff for participating in many useful discussions and for making suggestions concerning this work.

References

[1]Degani, D. and Schiff, L. B., "Numerical Simulation of the Effect of Spatial Disturbances on Vortex Asymmetry," AIAA Paper 89–0340, Jan. 1989.

[2]Bloor, S. M., "The Transition to Turbulence in the Wake of a Circular Cylinder," *Journal of Fluid Mechanics,* Vol. 19, 1964, pp. 290–304.

[3]Kourta, A., Boisson, H. C., Chassaing, P., and Minh, H. H., "Nonlinear Interaction and the Transition to Turbulence in the Wake of a Circular Cylinder," *Journal of Fluid Mechanics,* Vol. 181, 1987, pp. 141–161.

[4]Wei, T. and Smith C. R., "Secondary Vortices in the Wake of Circular Cylinders," *Journal of Fluid Mechanics,* Vol. 169, 1986, pp. 513–533.

[5]Poll, D. I. A., "Some Observations of the Transition Process on the Windward Face of a Long Yawed Cylinder," *Journal of Fluid Mechanics,* Vol. 150, 1985, pp. 329–356.

[6]Dexter, P. C. and Hunt, B. L., "The Effects of Roll Angle on the Flow Over a Slender Body of Revolution at High Angle of Attack," AIAA Paper 81-0358, Jan. 1981.

[7]Hunt, B. L. and Dexter, P. C., "Pressures on a Slender Body at High Angle of Attack in a Very Low Turbulence Level Airstream," *High Angle of Attack Aerodynamics,* AGARD-CP-247, Paper 17, 1978.

[8]Ericsson, L. E., "Vortex Unsteadiness on Slender Bodies at High Incidence," *Journal of Spacecraft,* Vol. 24, 1987, pp. 319–326.

[9]Gerich, D. and Eckelmann, H., "Influence of End Plates and Free Ends on the Shedding Frequency of Circular Cylinders," *Journal of Fluid Mechanics,* Vol. 122, 1982, pp. 109–121.